AIAA JOURNAL
Vol. 36, No. 6, June 1998

Numerical Study of Nozzle Exit Condition Effects on Jet Development

Thomas S. Chyczewski,* Lyle N. Long,† and Philip J. Morris‡
Pennsylvania State University, University Park, Pennsylvania 16802

Numerical predictions of the influence of nozzle exit conditions on the development of an ideally expanded supersonic rectangular jet are performed. The effects of these conditions on the jet's development have been found to be significant in experimental investigations. A model for the initial conditions is developed. A higher-order accurate finite difference algorithm for the solution of the full three-dimensional Navier–Stokes equations is used to generate results that isolate the impacts of excitation amplitude, modal excitation, and corner vortices on the jet character. Time-averaged, cross-correlation, and cross-spectral data are gathered from the simulation and compared to experimental data. The results indicate that, over the range of operating conditions considered here, the excitation amplitude does not significantly alter the jet development. The corner vortices, although prescribed in a sense that should anticipate axis switching (as determined by experimental subsonic results), are found to delay it. This appears to be caused by the dominance of flow instabilities in supersonic jets and the observed tendency of the corner vortices to reduce the mixing associated with this instability. Finally, independent of modal excitation, the lowest-order modes (of the large-scale turbulence structure) are found to consist of a combination of flapping in the minor axis plane with varicose motion in the major axis plane.

I. Introduction

EXPERIMENTAL, theoretical, and numerical investigations of high-speed jet flows have been undertaken by many researchers over the past 50 years. Motivated primarily by the development of the jet engine, these investigations have focused on improving our physical understanding of jet flows and the noise that they radiate with the ultimate goal of reducing the jet's annoyance. Recent changes in the Federal Aviation Administration's noise certification standards,[1] coupled with a national interest in the development of a high-speed civil transport, have compelled many researchers to revisit the jet noise problem and to develop prediction tools further.

Currently, there are three jet noise prediction strategies that have received the most attention: acoustic analogy methods,[2–4] instability wave methods,[5–8] and direct simulation (DS) methods.[9–11] In the acoustic analogy approach, the governing equations are recast into the form of an inhomogeneous wave equation, where the independent variable to which the wave operator is applied is some acoustic quantity and the forcing function can be interpreted as the noise sources of the flow. Instability wave methods are based on ample experimental evidence that it is the growth and decay of large, coherent turbulent structures in the shear layer that are the most efficient noise generators in high-speed jets.[12–14] These structures are modeled as instability waves, whose development is determined by a specified mean flow. A proper mathematical approach shows that under certain conditions, these instability waves radiate noise to the far field. Both the acoustic analogy and instability wave methods have their merits. They have significantly improved our understanding of jet noise and have provided scaling laws that have influenced aircraft engine design. However, their dependence on empirical data (the forcing function in the acoustic analogy and the mean flow in the instability wave methods) reduces their effectiveness as predictive tools.

With the advent of parallel processors and the promise of teraflop performance, the DS strategy is becoming more attractive. This approach requires the time-dependent numerical solution of the equations that govern both the flow and the acoustic field. Unlike the direct numerical simulation of turbulence, DS in the context of computational aeroacoustics problems for high-speed jets does not necessarily incorporate the resolution of all scales of the flow nor the direct simulation of the entire domain of interest, i.e., the acoustic far field. Instead, some assumptions can be made to simplify the problem. Because there is evidence that it is the large-scale coherent structures that are responsible for supersonic jet noise (a conclusion that is strengthened by the success of the instability wave methods), it appears reasonable to require that only these large scales be resolved by the grid. The effect of the small scales on the resolved scales is either accounted for through a subgrid-scale (SGS) turbulence model or is not addressed explicitly and is left to the numerical schemes' artificial dissipation to provide. The DS problem can be simplified further by reducing the size of the computational domain with the use of a Kirchhoff method.[15,16] The method consists of defining a surface within the computational domain that encloses the noise sources and does not intersect nonlinear flow regions. Given the time-dependent solution on this surface, the acoustic radiation can be determined at any location outside of the surface. Combined, the reduced resolution and computational domain size requirements relaxes the computing power needed for DS significantly.

The jet noise problem, however, introduces additional complexities. Even with the computational power available today, it is impractical to simulate the entire jet system (starting at, for example, a plenum chamber or combustor). Instead, a more feasible approach consists of confining the computational domain to a truncated region outside of the nozzle and modeling the flow that enters this domain from the nozzle exit. However, the characteristics of this modeled unsteady exit flow can have a significant effect on the jet flow that develops.

The effect of the initial conditions on experimental and numerically simulated jets have been studied by many investigators.[17–24] Hussain and Husain[17] found experimentally that the development of the subsonic jet depends on the nozzle boundary-layer momentum thickness distribution. The azimuthal variation has been shown by them to produce noticeable effects on the spreading rate of elliptic jets. These effects are the result of the influence of the momentum thickness on the generation of coherent structures. King et al.[21] found that nozzle imperfections as small as 0.2% of the nozzle exit diameter may have a significant effect on the development of supersonic axisymmetric jets. They used this information to develop methods of enhancing jet mixing. Quinn[23] found that facility differences resulted in changes in the spreading rate of two subsonic jets

Received Jan. 27, 1997; revision received Feb. 15, 1998; accepted for publication Feb. 25, 1998.

*Research Associate, Applied Research Laboratory. Member AIAA.
†Associate Professor, Department of Aerospace Engineering. Associate Member AIAA.
‡Boeing/A.D. Welliver Professor of Aerospace Engineering, Department of Aerospace Engineering. Associate Member AIAA.

operating under essentially the same flow conditions and geometry. Experimental evidence also indicates that vortices exist at each of the corners of asymmetric nozzles.[18,22,24] They are caused by azimuthal pressure gradients that form inside the nozzle as a result of varying flow accelerations along the different walls of the nozzle. These gradients skew the boundary layer and cause vortices to roll up in the corners.[25] They have been found to play a significant role in the axis switching phenomenon found in asymmetric jets.

This experimental evidence suggests that apparently minor differences in laboratory facilities can have an appreciable effect on the development of a jet. These effects can be observed in the form of varying potential core lengths, turbulence levels, and jet spreading rates. To compound this problem, the nozzle exit conditions of velocity and temperature of rectangular jets of engineering interest are too severe for today's measurement techniques to define precisely. This uncertainty, coupled with the numerical solution's sensitivity to the nozzle exit conditions, has lead us to develop a model for this flow and to study the effects of different initial features on the jet development. The basic numerical model and the evaluation of its predictive capability are reported in Ref. 26. This paper focuses on the results of evaluating the jet nozzle exit conditions influence on the developing jet.

The model is used in a high-resolution Navier–Stokes code to predict the ideally expanded cold supersonic flow issuing from a rectangular nozzle. The flow conditions ($M_{\text{jet}} = 1.54$, $Re_{\text{jet}} = 25{,}000$) and nozzle geometry (aspect ratio of 3) have been selected to match those of a parallel experimental investigation that has recently concluded at Pennsylvania State University.[27] Detailed information on the experimental setup, as well as experimental results, has been provided.

In our model, we rely on the numerical dissipation to behave like an SGS model. We did not perform a spectral analysis of the small-scale flow features, and so it is uncertain whether or not we are faithfully representing the turbulence. This should be kept in mind when interpreting the results. However, a comparison between the dissipation used in our model to the dissipation supplied by the Smagorinsky SGS model reveals that they behave similarly.[26]

The next section presents an overview of the numerical approach. This is followed by a detailed discussion of the nozzle exit boundary conditions. Next, jet simulation results obtained using these conditions are presented for a variety of cases designed to isolate the effect of each characteristic of the model. Whenever possible, comparisons are made with the corresponding experiment. Finally, some conclusions are drawn.

II. Overview of Numerical Approach

In this section, all pertinent aspects of the numerical approach except the nozzle exit boundary conditions are summarized. Details of the algorithm can be found in Ref. 26.

A supersonic rectangular jet flow is a nonlinear, viscous, unsteady, compressible, three-dimensional problem. As such, it is governed the full three-dimensional Navier–Stokes equations. These equations are solved in a time-accurate manner on a curvilinear coordinate system using high-order accurate finite difference approximations. The large-scale turbulent structures are resolved by the grid, whereas the effect of the small scales is accounted for through the numerical dissipation. Thus, no turbulence model is used. The code has been written in CM Fortran, which is a dialect of High Performance Fortran (HPF). It has been developed on the Thinking Machines CM-5 and has achieved very good parallel performance. Porting it to any computer with an HPF compiler (such as an IBM SP2, Silicon Graphics O2000, or Cray T3E) should be straightforward.

The numerical solution is advanced in time using a fourth-order accurate Runge–Kutta technique. This provides a high-order accurate time-integration scheme and requires no special startup treatment. It also has the advantage of a relaxed Courant–Friedrichs–Lewy (CFL) limit. A sixth-order accurate finite difference method is used to evaluate the spatial derivatives at the interior mesh points to minimize significant dissipation and dispersion errors to the resolved scales. This scheme requires a seven-point stencil, and special treatment at the first and last three grid points of the domain is necessary. In agreement with the work of Carpenter et al.,[28] it was found that an unstable scheme is produced if sixth-order accurate biased stencils are used at these boundary points. The scheme becomes stable if the first two grid points employ third-order accurate approximations, whereas fourth-order accurate approximation is used at the third grid point. The same pattern is used for the last three grid points.

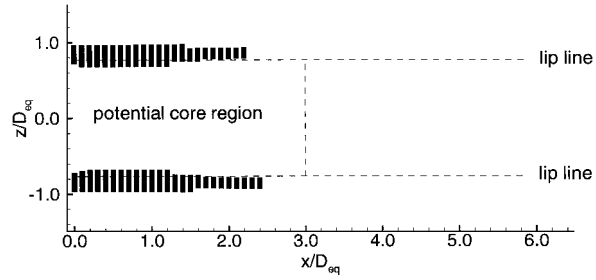

Fig. 1 Locations in the major axis plane where second-order dissipation is applied.

A combination of second- and sixth-order dissipation is used to stabilize the scheme. The sixth-order dissipation serves as a background filter, whereas the second-order dissipation is applied only in regions containing significant gradients. Figure 1 is a scatter plot of the locations where the second-order dissipation is turned on in a plane that passes through the jet centerline for a typical calculation. These locations are found to be confined to the jet shear layer in the potential core region. These locations are roughly the same region where an SGS model would be activated.

The nonreflecting boundary conditions proposed by Thompson[29] are implemented to minimize nonphysical reflections at the far-field boundaries. The primitive form of these equations are used. The method decomposes the nonlinear Euler equations into wave modes of definite velocity and enforces a nonreflecting condition for those modes that have a velocity directed into the domain. The performance of these conditions is augmented in this work by stretching the grid slightly and providing second-order dissipation near the boundaries. This approach has proven quite effective in reducing the amplitude of reflected waves, as also shown in other studies.[10] The downstream exit plane is located $30D_{\text{eq}}$ away from the nozzle exit. We found that this distance allows the natural and artificially imposed decay mechanisms of the instabilities to reduce the instability amplitudes to levels that can be handled by the boundary conditions with little reflection. Moving the outflow boundary farther downstream had little effect on the instability wave growth and decay.

III. Nozzle Exit Boundary Conditions

The computational domain begins at the nozzle exit. Thus, the nozzle exit conditions are prescribed at the plane in which the flow leaves the nozzle. The remainder of the jet exit plane is treated as a solid wall. We, therefore, avoid the possibility of exciting the jet with far-field boundary conditions that are not accurate near the jet. This is done at the expense of modifying ambient fluid entrainment. To some degree, however, this more closely reproduces the conditions of the experiment we attempt to simulate, which was conducted inside a small anechoic chamber. The nozzle exit plane was located 5–10 equivalent diameters away from the chamber wall.

A complete prescription of the nozzle exit conditions requires the specification of both steady and unsteady spatial and temporal characteristics. They are described in the following two subsections.

A. Steady Nozzle Conditions

The steady-state nozzle exit conditions are prescribed following the experimental data.[27] These data indicate that viscous effects are confined to locations very close to the nozzle wall. Thus, the simulated jets use uniform profiles for density, axial velocity, and pressure. Numerically, enforcing tophat profiles may lead to a numerically induced instability. However, these profiles make up only the steady component. The instantaneously prescribed condition consists of contributions from both the steady and unsteady models. The unsteady contribution has a smooth spatial distribution, which decreases the impact of the sharp steady profile. This has been verified by examination of frequency spectra at small distances downstream

of the nozzle exit. Clearly, these profiles also do not account for possible azimuthal momentum thickness variations that may exist around the nozzle lip. The absence of experimental data compels this simplification.

Because the nozzle exit flow is supersonic, characteristic theory requires that all five independent variables be specified. The two remaining variables are the components of velocity parallel to the nozzle exit plane. A pitot probe aligned with the jet axis was used by the experimentalists to determine the exit Mach number. This measures only the axial component of the velocity. Whether or not crossflow velocities exist in the experimental jet or their magnitude is unknown. Two possibilities for the behavior of the crossflow velocities are considered in our model. One is to simply set them to zero and have a purely axial initial mean flow. The other possibility is to specify these variables such that they are consistent with the velocity induced by vortices located near the corners of the nozzle. Both possibilities are considered.

In the corner vortex cases, the crossflow velocities are determined by calculating the velocity induced by the superposition of four ideal vortices, one near each corner of the nozzle cross section. The sense of each vortex in the model is chosen such that axis switching should be promoted (based on the results of Zaman[24]). In this case, the counter-rotating vortex pairs on opposite sides of the minor axis plane will tend to inject ambient fluid through the short sides of the cross section and to expel jet flow through the long sides. Vortices with the same sense as these were generated in Zaman's experiment[24] by placing delta tabs on the short dimension of the nozzle walls at the exit. The magnitude of the vorticity is specified here such that the maximum crossflow speed is equal to 1/10th of the axial velocity.

B. Unsteady Nozzle Conditions

There is a very limited amount of information available in the literature that discusses the unsteady features of a supersonic nozzle exit flow. This lack of published information has been overcome in the current research by a close interaction with the experimentalists who conducted the laboratory tests of the rectangular jet. This interaction has lead to the development of a set of unsteady nozzle exit conditions that specify the disturbance spatial distribution, amplitude, temporal behavior, and phase relation around the nozzle lip. By controlling the phase relation, different modes (flapping or varicose) can be excited at the nozzle exit. This is similar to the artificial excitation used by many experimentalists.[27,30–33]

The velocity perturbations are calculated from the following relation:

$$u',\ v',\ \text{or}\ w' = \frac{u_j}{2}\alpha \sum_{i=1}^{4} c_i A_i \sum_{l=1}^{2} \sin\left(2\pi f_l t + \phi_l^n + \beta_i\right) \qquad (1)$$

These terms are defined in the following sections.

1. Temporal Behavior

The inner summation in Eq. (1) is over contributions from two characteristic frequencies. These two frequencies are the screech tone frequencies found in the minor axis plane of the experimental jet.[27] These frequencies can also be determined using the linear shock cell model and weakest link theory developed by Tam.[34] For our problem, they are $f_1 = 9606$ Hz and $f_2 = 26{,}367$ Hz. The corresponding Strouhal numbers are 0.31 and 0.84, respectively. The Strouhal number is defined here as the frequency nondimensionalized by the exit velocity and the equivalent diameter of the experimental jet.

A random component to the excitation is supplied by ϕ_l^n in Eq. (1). It is initialized to zero at the beginning of each run. It is then updated at each time step n by the following expression:

$$\phi_l^n = \phi_l^{n-1} \pm \theta \qquad (2)$$

The amplitude of the phase shift between time steps θ is 5.4 deg. This value was found to give the favorable characteristics to be described. Whether the phase is increased or decreased by θ is determined in a random manner and may differ between ϕ_1^n and ϕ_2^n. Thus, the contributions of the two characteristic frequencies are generally not in phase.

The effect of supplying a random phase shift, called a random walk,[35] is to make the frequency spectrum broadband, as opposed to the discrete spectrum associated with simple harmonic excitation. The band of energy-containing frequencies is controlled by θ and the two characteristic frequencies f_1 and f_2. The value of θ is selected so that the upper limit of the energy-containing frequencies occurs near the limit frequency that the scheme and the grid can resolve.[26] Thus, a minimal amount of the energy supplied by the boundary condition is damped by the numerical scheme. In contrast, if a purely random excitation is used, much of the energy content would be above the limit frequency and, consequently, much of the input perturbation would be damped.

2. Spatial Distribution

The perturbation on the entire nozzle lip is determined by building it up from the contributions of the four walls. This is done in Eq. (1) by the outer summation. A_i is the spatial amplitude function for each of the walls. Indices 1 and 3 refer to the long walls (contained in the major axis plane), whereas indices 2 and 4 refer to the short walls (contained in the minor axis plane). The amplitude distribution normal to the nozzle wall is a Gaussian function centered on the lip line of each wall. The half-width of the Gaussian is 1/10th of the short dimension of the nozzle. The function is tapered to zero amplitude near the corners of the nozzle. This spatial function is selected inasmuch as a Gaussian is a representative distribution for wall bounded shear layer perturbations (see Ref. 27, for example).

3. Mode Excitation

Two different modal excitations are considered in our model. These are the varicose and flapping modes that have been found in the experiment.[27] The varicose mode is characterized by symmetric shedding of coherent structures from the nozzle lip, whereas the vortex shedding is asymmetric for the flapping jet case. These different modes are excited in the jet by controlling phase differences between the walls of the nozzle. The phase difference is controlled by the angle β_i in Eq. (1). Whether or not there is a velocity component contribution to the perturbation from a wall is determined by the parameter c_i. The values of these two parameters for each of the velocity components is given for the varicose excitation as

$$u'\colon c_{1-4} = 1, \qquad \beta_{1-4} = 0$$
$$v'\colon c_{1,3} = 1, \qquad c_{2,4} = 0, \qquad \beta_1 = \pi/2$$
$$\beta_{2,4} = 0, \qquad \beta_3 = -(\pi/2)$$
$$w'\colon c_{1,3} = 0, \qquad c_{2,4} = 1, \qquad \beta_{1,3} = 0,$$
$$\beta_2 = -(\pi/2), \qquad \beta_4 = \pi/2$$

and for the flapping excitation as

$$u'\colon c_{1,3} = 1, \qquad c_{2,4} = 0, \qquad \beta_{1,2,4} = 0, \qquad \beta_3 = \pi$$
$$v'\colon c_{1,3} = 1, \qquad c_{2,4} = 0, \qquad \beta_1 = \pi/2$$
$$\beta_{2,4} = 0, \qquad \beta_3 = \pi/2$$
$$w'\colon c_{1-4} = 0, \qquad \beta_{1-4} = 0$$

The coordinate system is shown in Fig. 2. The major axis plane is aligned with the z axis, and (u, v, w) are the x, y, and z components of velocity, respectively.

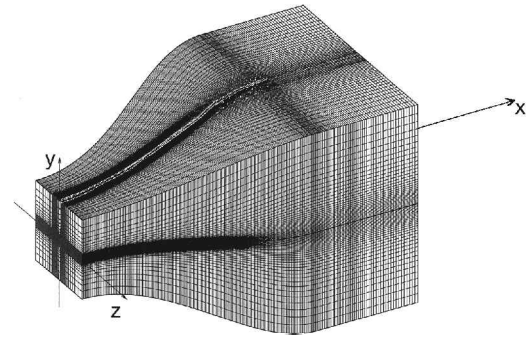

Fig. 2 Three-dimensional view of the grid (256 × 64 × 64).

The final parameter in Eq. (1) to be defined is α. It specifies the peak amplitude of the velocity perturbation. Two values (0.01 and 0.02) have been used to compare its effect on the jet's development. These values correspond to rms fluctuation levels near 0.70 and 1.36% of the exit velocity, respectively. The rms levels vary slightly from run to run due to the random nature of the excitation.

The instantaneous velocities are obtained by adding the steady contribution to the perturbation. Given these velocities, the pressure and density are found from conditions of constant total temperature and entropy. The first condition has been found to be reasonable for a jet flow under these conditions by Troutt and McLaughlin.[13] The assumption of isentropic excitation is justified because these perturbations most likely originated from acoustic disturbances upstream of the nozzle exit.

A test matrix of combinations of the options just discussed is given as case 1: corner vortices, varicose excitation, and $\alpha = 0.01$; case 2: corner vortices, varicose excitation, and $\alpha = 0.02$; case 3: no corner vortices, varicose excitation, and $\alpha = 0.02$; and case 4: no corner vortices, flapping excitation, and $\alpha = 0.02$. These combinations are selected to isolate the effects of each of the features of the nozzle conditions.

IV. Results

The supersonic rectangular jet flowfields predicted by the numerical scheme are presented in this section. The effects of the different nozzle exit conditions are analyzed, and a detailed comparison is made with experimental data taken by Kinzie.[27] The comparisons include time-averaged and unsteady quantities. The grid used in these calculations is shown in Fig. 2. It consists of 256 points in the axial direction and 64 points in each of the lateral directions. The outflow plane is $30D_{eq}$ from the nozzle exit plane. The lateral boundaries are $4D_{eq}$ from the jet centerline and spread to $10D_{eq}$ by the outflow plane.

A. Data Collection

Based on the conclusions drawn from a Fourier stability analysis,[26] the maximum CFL number in the domain is limited to 0.6. This occurs near the nozzle exit just outside of the jet. The CFL numbers in the jet shear layer and jet core are 0.55 and 0.16, respectively. These CFL numbers correspond to a constant time step of 3.0×10^{-7} s (based on the 13.8-mm equivalent diameter and 343.0-m/s ambient acoustic speed found in Ref. 27).

A complete run is made up of two phases. Because the initial condition of the simulation is a quiescent fluid, one phase is required to allow initial transients to leave the domain and to establish the jet. A sufficient number of steps for this phase is estimated by considering the number of cycles a low-frequency wave can achieve in this period. Running the code for 33,000 steps, using the time step given earlier, corresponds to 0.01 s of time. In terms of cycles of the lower frequencies, this amount of time allows a signal with a wavelength of one equivalent jet diameter to reach an axial location of $20D_{eq}$ and pass through 225 cycles. The solution is checked at this time to verify that all transients have left the domain and that the jet appears established.

The second phase is to sample variables in the major and minor axis planes that pass through the jet centerline. These data are used to determine time-average quantities and the cross-spectral information presented here. A sample over 32,768 time steps is used. This number of steps (an integer power of 2 for Fourier analysis purposes) allows 31 cycles of a Strouhal number 0.1 disturbance to pass through any given location. The analysis presented in Coleman and Steele[36] was used to estimate the errors associated with calculating the mean of a stochastic variable from a finite sample of that variable. For our analysis, we calculate the error estimate of the mass flux along a line parallel to the jet axis that orginates at the midpoint of one of the major lip lines. The results are plotted in Fig. 3. Clearly, the errors associated with the finite sample are quite small for all of the axial stations presented here. We assume similar trends for the other time-averaged variables.

B. Time-Average Results

Figure 4 shows the centerline velocity distribution for cases 1–4 and compares them to the experimental data. The simulation results

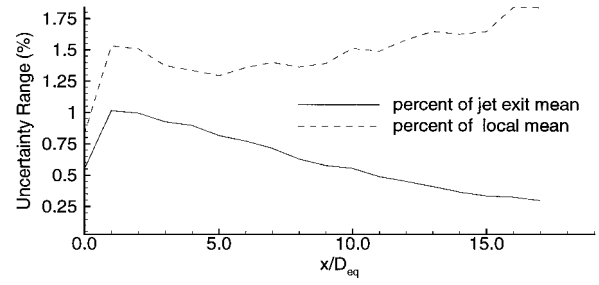

Fig. 3 Axial variation of the uncertainty in the mean value of the mass flux.

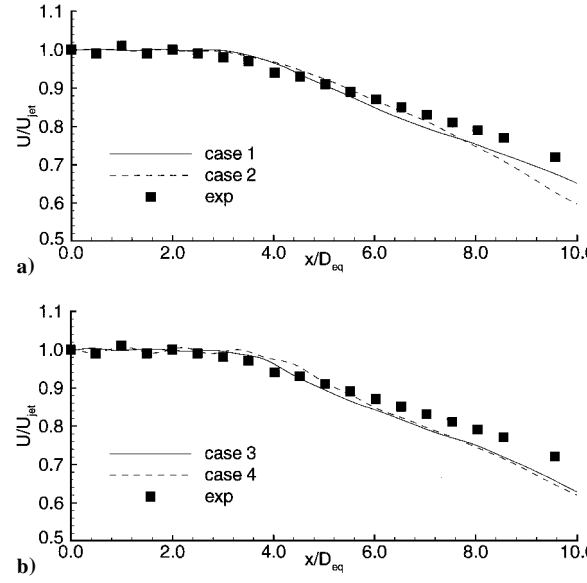

Fig. 4 Centerline velocity distributions for cases 1–4.

are shifted $-2D_{eq}$ for cases 1–3 to match the potential core length of the experiment (case 4 requires no shift). This shift is applied so that the decay rates of the centerline velocity can be compared directly and is used for all comparisons with experimental data presented throughout (for cases 1–3 only).

The two simulation profiles shown in Fig. 4a isolate the effect of different nozzle perturbation amplitudes. There are no clearly distinguishing features between these profiles. This is most likely associated with the zero momentum thickness profile that is prescribed at the nozzle exit, which will lead to a very high-instability growth rate independent of excitation amplitude. The comparisons between the simulations and experiments after the end of the potential core show that the simulation overpredicts the turbulent mixing slightly for both nozzle conditions inasmuch as their centerline velocities decay at a faster rate.

The turbulent mixing is even more rapid in cases 3 and 4, which have nearly identical decay rates as shown in Fig. 4b. Comparing the two cases with corner vortices (Fig. 4a) to the two cases without corner vortices (Fig. 4b), the centerline profiles suggest that the corner vortices are reducing the mixing in the turbulent jet.

One of the distinguishing features between cases 3 and 4, where the difference is in the modal excitation of the nozzle exit, is that the flapping excitation case 4 has noticeable oscillations in the potential core region. These oscillations, also present in the experimental data, are due to a weak shock cell structure. They are also present to a lesser degree in the case 3 profiles and virtually absent in cases 1 and 2. In the experimental jet, this structure most likely originates in the throat of the nozzle as a result of an imperfect nozzle design.

Recall that the static pressure prescribed by the steady nozzle exit conditions is set to the ambient pressure for all of the cases; however, superimposed on this steady condition are perturbations. These perturbations are likely responsible for the weak shock cell structure found in the simulated jet. Why the flapping mode excitation produces a stronger shock cell structure is not understood;

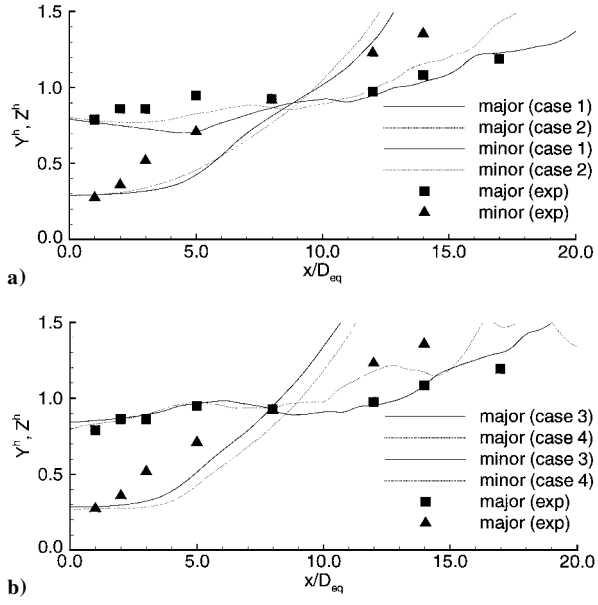

Fig. 5 Velocity half-thicknesses for cases 1–4.

however, it is interesting to note that the simulation reproduces fairly accurately the amplitude, wavelength, and phase of the shock cell structure (given the limited resolution of the experimental data).

Figure 5 shows the velocity half-thicknesses of the jet in the major and minor axis planes for the four nozzle exit conditions and compares them to the experimental data. This thickness is defined as the lateral distance (in the major or minor axis planes) from the jet centerline to the point in the profile where the velocity is reduced to half the local centerline velocity. Considering, first, the major axis thicknesses, the comparison for all of the simulation cases with the experiment is quite good.

The effect of the corner vortices is most pronounced in cases 1 and 2, where there is a noticeable decrease in the velocity half-thickness early in the jet development. Recall that the sense of the vortices in the model is chosen to anticipate an axis switch. Thus, in terms of the half-thickness parameter, the vortices should reduce the half-thickness in the major axis plane and cause a higher growth rate of the half-thickness in the minor axis plane. This effect is observed in the major axis. It appears to be more pronounced for case 1, where the initial amplitude of the perturbations at the nozzle exit is lower.

The initial reduction of the major axis half-thickness is not observed in Fig. 5b, which shows the cases where the corner vortices have been turned off. The comparison with the experimental data is improved for these cases, suggesting the absence or weakness of the nozzle exit corner vortices in the experiments.

As for the half-thickness parameter in the minor axis plane, the simulation underpredicts the growth rate early in the jet development. This is even true when the corner vortices are included, which should increase the minor axis half-thickness growth rate. Similar to the major axis plane, the corner vortices are expected to have a more pronounced effect early in the jet's development. Instead, for the minor axis, their effect is not observed until after the end of the potential core and, in fact, slightly reduces the growth rate in the minor axis plane.

The jet growth rate in the minor axis plane is larger for the simulated jet compared to the experimental results in all cases at larger distances from the nozzle exit. We suspect that this is because the growth of the experimental jet was inhibited by the proximity of the facility walls to the jet centerline ($20D_{eq}$) and because the jet exhausts the anechoic chamber through a diffuser.

Because, early in the jet development, the major axis thickness growth is less than that of the minor axis and is fairly independent of the nozzle exit conditions, the growth rate of the minor axis half-thickness has a more significant role in fixing the axis switch location. Recall that the axis switch location is the axial station where the half-thickness in the minor axis plane equals that in the major axis. A comparison of the growth rates for all of the cases reveals that the modal excitation can be as influential as the corner vortices in the determination of the axis switch location. In fact, specification of these vortices in the sense suggested by Zaman[24] to anticipate axis switching actually delays it by about $0.5D_{eq}$.

This inconsistent behavior is likely due to the difference in conditions between Zaman's experiment,[24] which focused on subsonic rectangular jets, and the simulations presented here. Although Zaman postulates that the effect of the delta tabs is the same for supersonic jets as it is for subsonic ones, the evidence provided by the simulations suggests that, for supersonic jets, the flow instability effects dominate the dynamics of the flow in the minor axis plane, thus reducing the effectiveness of the corner vortices. In addition, the simulations indicate that, for supersonic jets, the effect of the corner vortices is to reduce mixing in the minor axis plane (based on Fig. 5) and, consequently, delay the axis switch. Other factors that may contribute to the discrepancy between our results and those of Zaman[24] include the strength of the vortices and the amplitude of the modal excitation prescribed by the boundary conditions. The coherence of the excitation may also play a role in making the instability a very efficient mixing mechanism.

The observations made here of the axis switch location's dependence on the mixing in the minor axis plane is consistent with the work of Krothapalli et al.,[37] who compared the mixing of various supersonic jets with different pressure ratios. They found that the pressure ratio significantly influences the mixing in the minor axis plane and can have a significant effect on the location of an axis switch. These observations were attributed to the effect of shock cells on the jet instability. Similar observations were made by Gutmark et al.[38] In general, these shock cells also lead to a screech mechanism, which will make the ring vortices emanating from the nozzle more organized and effective at causing and axis switch (according to the ω_θ dynamics analysis of Zaman[24]). The jet simulations in this paper excited by a flapping mode do show a shock cell structure, but it is much weaker than the one found in Ref. 37. The presence of screech in the experimental data and its absence in the simulation most likely account for the earlier axis switch in the experiment compared to the no corner vortex simulation case.

C. Eddy Convection Speed

The results of an instability wave analysis suggest that the speed at which large-scale structures travel in the jet shear layer has a significant impact on the noise radiation efficiency of these structures.[8] This section presents the convection speeds predicted by the simulation and compares them to the experimental data.

At a particular location, the eddy convection speed can be determined by cross correlating the axial component of the mass flux between different axial locations. The cross correlation is defined as

$$R_{ab}(x, \Delta, \tau) = \frac{1}{t_2 - t_1} \int_{t_1}^{t_2} V_a(x, t) V_b(x + \Delta, t + \tau)\, \mathrm{d}t \qquad (3)$$

where, for our purposes, V_a and V_b are defined as ρu.

The delay time at which the cross correlation becomes maximum for a given Δ can be interpreted as the time required by an eddy to travel from x to $x + \Delta$. Thus, the convection speed can be determined by dividing the spatial separation by $\tau_{R_{\max}}$. The eddy convection speeds, normalized by the jet exit velocity, are shown in Fig. 6 for the varicose (case 3) and flapping (case 4) excitation nozzle exit conditions.

In the potential core region for the varicose excitation case (Fig. 6a) the convection speed in both the major and minor axis planes is nearly identical with a value of $0.68U_j$. After the end of the potential core there is a slight increase in convection speed in the minor axis plane, whereas the major axis plane convection speed decreases monotonically.

Kinzie[27] calculated the convection speed of the large-scale structures in an elliptic jet excited at a Strouhal number of 0.4. These speeds were calculated by evaluating the cross spectra between the excitation and a hot wire located at different axial locations in the shear layer. The change in phase with axial location revealed the wavelength of the structure from which the convection speed could be determined given the excitation frequency. Kinzie[27] notes, however, that the uncertainty in his results are high due to the

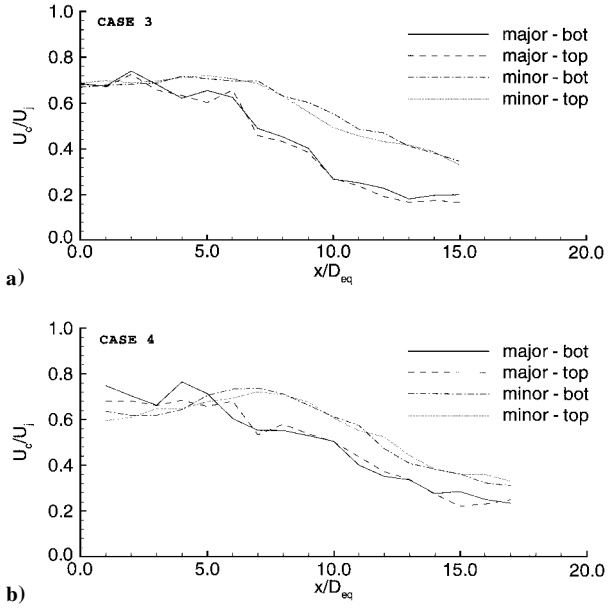

Fig. 6 Structure convection speed for cases 3 and 4.

significant variation of phase with radial position. For varicose excitation, downstream of the end of the potential core, Kinzie found that the convection speed of the structures is $0.77U_j$.

Unlike the varicose excitation case, there is a significant difference in the convection speed between the major and minor axes in the potential core region for the flapping excitation case. The major axis convection speed remains near $0.68U_j$, but the minor axis speed is reduced to about $0.61U_j$. Like the varicose excitation case, however, the convection speed in the minor axis does accelerate to a peak speed near $0.7U_j$. Thus, it appears as though the major axis plane structure speed is independent of the modal excitation. The minor axis plane, on the other hand, shows some variation in the potential core region with excitation mode. In the next section, cross spectral data are presented that suggest that for the major axis plane a varicose mode is the preferred mode, whereas for the minor axis plane a flapping mode is the preferred mode. This is true for both the flapping and varicose mode excitation cases. According to the results of Morris and Bhat,[8] the structure speed in a jet in a varicose mode is faster than that of a flapping jet. Thus, considering the preferred mode for each axis plane, this is consistent with the observations of faster convection speeds in the major axis plane compared to the minor axis plane (in the potential core region).

D. Jet Instability Modes

In Fig. 7 the phase difference and coherence of the ρu signals on bottom and top lip lines in the minor axis plane are shown for the varicose excitation case. Recall that for a varicose excitation these signals should be in phase. This appears as a straight line at $\theta_{BT} = 0$ in the figure. Also, the coherence between these two signals is 1.0.

Aside from a drop in coherence near $Sr = 0.1$, there is not much change as the jet develops between the nozzle exit and $1D_{\text{eq}}$. At $3D_{\text{eq}}$, however, there is a 180-deg phase difference between the two signals at the low frequencies (below $Sr = 0.2$). The coherence has also retained a high level in this region. As the flow develops further, the phase difference spreads to most of the frequency range; however, the coherence is reduced, which reduces the validity of the phase data. The phase shift across the minor axis plane is consistent with the flapping mode of the jet. Cross-spectral phase and coherence data in the major axis plane indicates that the major axis plane maintains a varicose motion.[26]

The cross-spectra phase and coherence of ρu in the major axis plane for the flapping excitation is shown in Fig. 8. For the flapping mode excitation, there are no velocity perturbations imposed on the lip lines of the short dimension of the nozzle. As the jet develops, however, ρu perturbations are generated and are in phase between the top and bottom lip lines. This is consistent with a varicose motion. Cross-spectral phase and coherence data in the minor

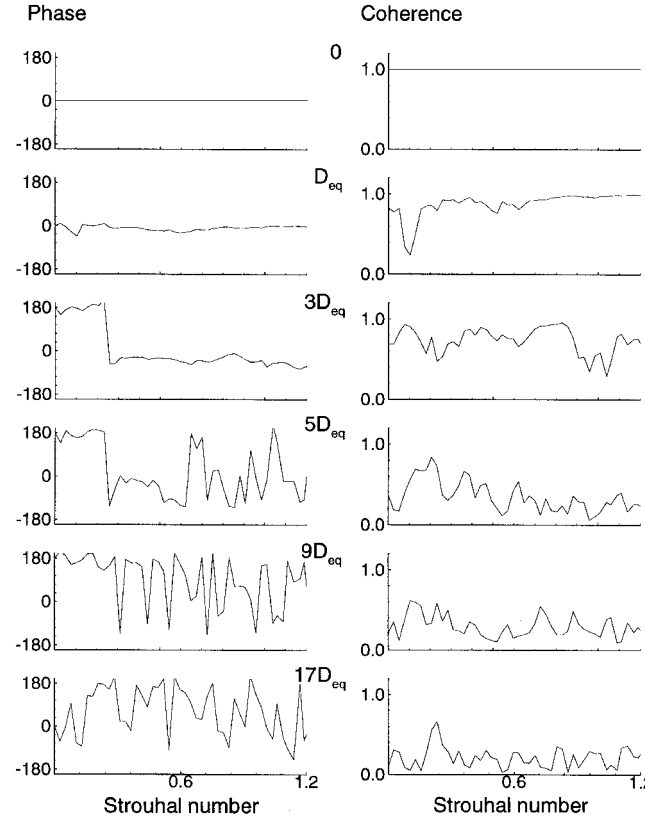

Fig. 7 Cross-spectra phase and coherence of ρu between the top and bottom lip lines of the minor axis plane for the varicose excitation case (case 3). The number to the right of each phase graph indicates axial location for it and the adjacent coherence graph.

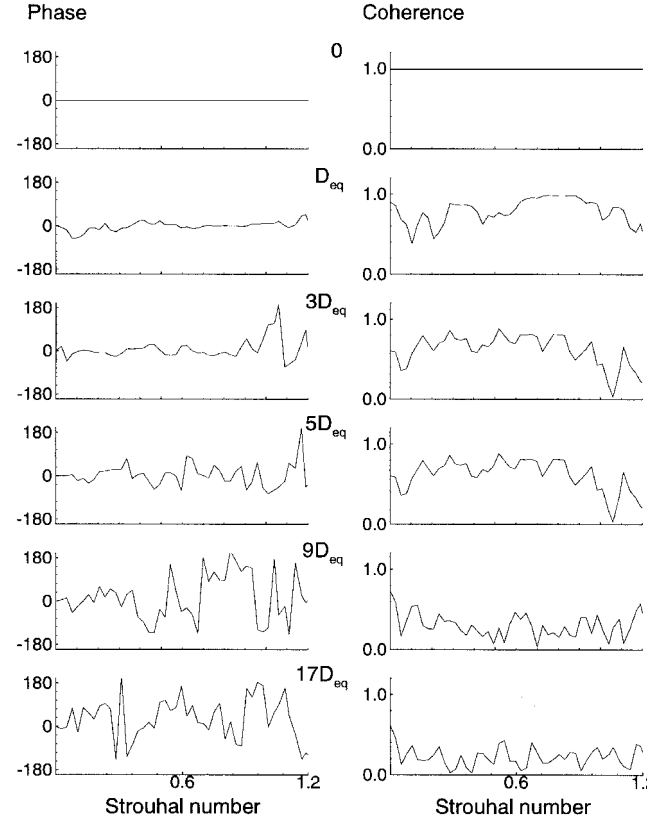

Fig. 8 Cross-spectra phase and coherence of ρu between the top and bottom lip lines of the major axis plane for the flapping excitation case (case 4). The number to the right of each phase graph indicates axial location for it and the adjacent coherence graph.

axis plane indicate that the minor axis plane maintains a flapping motion.[26] Thus, independent of jet excitation, it appears as though for the minor axis plane a flapping mode is the preferred mode and for the major axis plane a varicose mode is the preferred mode.

It is difficult to obtain experimental verification of these jet instability observations from the experimental data. However, Kinzie[27] was able to perform a modal decomposition of the acoustic field. These results suggest that a varicose mode dominates the acoustic field, although there is some flapping present. This might suggest that for the experimental jet a varicose mode is preferred, but this is not conclusive because there is no evidence that there is a direct correlation between the modes of a jet and the acoustic modes in the far field. In other studies of imperfectly expanded jets, there is ample evidence that the presence of a shock cell structure in the jet plume causes a severe flapping motion to occur in the minor axis plane.[37–39] This was found to a dependent on the strength of the shocks in the jet plume.

The conclusions drawn in this section explain some of the observations made earlier. Aside from helping to interpret the structure convection speed predictions discussed in the preceding section, some of the results of the time-average data may be explained. In particular, referring to Fig. 4, where the effects of mode excitation on the centerline velocity distribution are shown, the velocity decay rate between the different excitation modes is nearly identical. This suggests similar mixing mechanisms. Recall also that for the varicose excitation cases a shift of $-2D_{eq}$ is required to match the potential core length of the experimental data. No such shift is required for the flapping excitation case. The extra $2D_{eq}$ required by the varicose simulation may be explained by the spatial development region required to transition the varicose mode in the minor axis plane to a flapping mode.

V. Conclusions

A model for the flow leaving the nozzle of a supersonic jet is presented and used within a high-resolution finite difference algorithm for the solution of the full Navier–Stokes equations to predict the effects of various experimentally observed exit flow characteristics on the development of an ideally expanded rectangular jet. These characteristics include excitation amplitude, modal excitation, and the possible existence of corner vortices.

Our results indicate that the influence of the excitation amplitude, in the range investigated, is relatively small. This result is attributed to tophat mean profiles prescribed at the nozzle exit. The effect of the nozzle corner vortices in our supersonic jet simulations has been found to differ from that of an experimentally studied subsonic jet. Instead of anticipating axis switching, the corner vortices with the sense specified here delay axis switching by about $0.5D_{eq}$. Unlike the subsonic jet thickness growth, which is dominated by vortex dynamics, the supersonic jet thickness growth is dominated by the mixing due to flow instability. This mixing appears to be reduced by the corner vortices, thus delaying the axis switch. Our results also suggest that the major and minor axis planes have a preferred instability mode. Independent of the excitation, the minor axis plane exhibits a flapping motion, whereas for the major axis plane a varicose motion is preferred.

Acknowledgments

This work was funded by the NASA Graduate Student Research Program and by NASA Grants NAG-1-1479 and NAG-1-1367. Computer resources were provided by the NASA Numerical Aerodynamic Simulation Program and by the National Center for Supercomputing Applications. The authors would like to acknowledge the helpful suggestions of D. K. McLaughlin and K. Kinzie in this study.

References

[1]"Noise Standards for Aircraft Type Certification (Modifications to FAR Part 36)," U.S. Environmental Protection Agency, EPA 550/9-76-013, 197, Washington, DC, 1994.

[2]Lighthill, M. J., "Jet Noise," *AIAA Journal*, Vol. 1, No. 7, 1963, pp. 1507–1517.

[3]Ribner, H. S., "Quadrupole Correlations Governing the Pattern of Jet Noise," *Journal of Fluid Mechanics*, Vol. 38, 1969, pp. 1–24.

[4]Goldstein, M. E., *Aeroacoustics*, McGraw–Hill International, New York, 1975, Chap. 2.

[5]Tam, C. K. W., and Morris, P. J., "The Radiation of Sound by the Instability Waves of Compressible Plane Turbulent Shear Layers," *Journal of Fluid Mechanics*, Vol. 98, May 1980, pp. 349–381.

[6]Tam, C. K. W., and Burton, D. E., "Sound Generated by Instability Waves of Supersonic Flows. Part 2. Axisymmetric Jets," *Journal of Fluid Mechanics*, Vol. 138, Jan. 1984, pp. 273–295.

[7]Tam, C. K. W., Chen, P., and Seiner, J. M., "Relationship between Instability Waves and Noise of High Speed Jets," *AIAA Journal*, Vol. 30, No. 7, 1992, pp. 1747–1752.

[8]Morris, P. J., and Bhat, R. T. S., "The Spatial Stability of Compressible Elliptic Jets," *Physics of Fluids*, Vol. 7, No. 1, 1995, pp. 185–194.

[9]Tam, C. K. W., and Webb, J. C., "Dispersion-Relation-Preserving Finite Difference Schemes for Computational Physics," *Journal of Computational Physics*, Vol. 107, No. 2, 1993, pp. 262–281.

[10]Colonius, T., Lele, S. K., and Moin, P., "Boundary Conditions for Direct Computation of Aerodynamic Sound Generation," *AIAA Journal*, Vol. 31, No. 9, 1993, pp. 1574–1582.

[11]Mitchell, B. E., Lele, S. K., and Moin, P., "Direct Computation of the Sound Generated by Subsonic and Supersonic Axisymmetric Jets," Thermosciences Div., Dept. of Mechanical Engineering, Rept. No. TF-66, Stanford Univ., Stanford, CA, 1995.

[12]Armstrong, R. R., Michalke, A., and Fuchs, H. V., "Coherent Structures in Jet Turbulence and Noise," *AIAA Journal*, Vol. 15, No. 7, 1977, pp. 1011–1017.

[13]Troutt, T. R., and McLaughlin, D. K., "Experiments on the Flow and Acoustic Properties of a Moderate Reynolds Number Supersonic Jet," *Journal of Fluid Mechanics*, Vol. 116, March 1982, pp. 123–156.

[14]Seiner, J. M., McLaughlin, D. K., and Liu, C. H., "Supersonic Jet Noise Generated by Large-Scale Instabilities," NASA TP 2072, 1982.

[15]Lyrintzis, A. S., "Review: The Use of the Kirchhoff's Method in Computational Aeroacoustics," *Journal of Fluids Engineering*, Vol. 116, No. 4, 1994, pp. 665–676.

[16]Özyörük, Y., and Long, L. N., "A Navier–Stokes/Kirchhoff Method for Noise Radiation from Ducted Fans," *AIAA Journal*, Vol. 34, No. 5, 1996, pp. 894–901.

[17]Hussain, F., and Husain, H. S., "Elliptic Jets. Part 1. Characteristics of Unexcited and Excited Jets," *Journal of Fluid Mechanics*, Vol. 208, Nov. 1989, pp. 257–320.

[18]Grinstein, F. F., "Vorticity Dynamics in Spatially Developing Rectangular Jets," AIAA Paper 93-3286, July 1993.

[19]Rice, E. J., and Raman, G., "Enhanced Mixing of a Rectangular Supersonic Jet by Natural and Induced Screech," AIAA Paper 93-3263, July 1993.

[20]Grinstein, F. F., Gutmark, E., and Parr, T., "Numerical and Experimental Study of the Near Field of Subsonic, Free Square Jets," AIAA Paper 94-0660, Jan. 1994.

[21]King, C. J., Krothapalli, A., and Strykowski, P. J., "Streamwise Vorticity Generation in Supersonic Jets with Minimal Thrust Loss," AIAA Paper 94-0661, Jan. 1994.

[22]Zaman, K. B. M. Q., "Effect of 'Delta Tabs' on the Mixing and Axis Switching in Jets from Axisymmetric Nozzles," AIAA Paper 94-0186, Jan. 1994.

[23]Quinn, W. R., "Turbulent Mixing in a Low Aspect Ratio Rectangular Jet," AIAA Paper 95-2148, June 1995.

[24]Zaman, K. B. M. Q., "Axis Switching and Spreading of an Asymmetric Jet—Role of Vorticity Dynamics," AIAA Paper 95-0889, Jan. 1995.

[25]Bradshaw, P., "Turbulent Secondary Flows," *Annual Review of Fluid Mechanics*, Vol. 19, 1987, p. 53.

[26]Chyczewski, T. S., "A Time-Dependent, Three-Dimensional Numerical Study of Supersonic Rectangular Jet Flow and Noise Using the Full Navier–Stokes Equations," Ph.D. Thesis, Dept. of Aerospace Engineering, Pennsylvania State Univ., University Park, PA, May 1996.

[27]Kinzie, K. W., "Aeroacoustic Properties of Moderate Reynolds Number Elliptic and Rectangular Supersonic Jets," Ph.D. Thesis, Dept. of Aerospace Engineering, Pennsylvania State Univ., University Park, PA, May 1995.

[28]Carpenter, M. H., Gottlieb, D., and Abarbanel, S., "Stable and Accurate Boundary Treatments for Compact, High-Order Finite-Difference Schemes," *Applied Numerical Mathematics*, Vol. 12, No. 12, 1993, pp. 55–87.

[29]Thompson, K. W., "Time-Dependent Boundary Conditions for Hyperbolic Systems, II," *Journal of Computational Physics*, Vol. 89, No. 2, 1990, pp. 439–461.

[30]McLaughlin, D. K., Morrison, G. L., and Troutt, T. R., "Experiments on the Instability Waves in a Supersonic Jets and Their Acoustic Radiation," *Journal of Fluid Mechanics*, Vol. 69, May 1975, pp. 73–95.

[31]McLaughlin, D. K., Morrison, G. L., and Troutt, T. R., "Reynolds Number Dependence in Supersonic Jet Noise," *AIAA Journal*, Vol. 15, No. 7, 1977, pp. 526–532.

[32]Troutt, T. R., "Measurements on the Flow and Acoustic Properties of a Moderate Reynolds Number Supersonic Jet," Ph.D. Thesis, Dept. of Mechanical and Aerospace Engineering, Oklahoma State Univ., July 1978.

[33]Morrison, G. L., and McLaughlin, D. K., "Noise Generated by Instabilities in Low Reynolds Number Supersonic Jets," *Journal of Sound and Vibration*, Vol. 65, No. 2, 1979, pp. 177–191.

[34]Tam, C. K. W., "The Shock-Cell Structures and Screech Tone Frequencies of Rectangular and Non-Axisymmetric Supersonic Jets," *Journal of Sound and Vibration*, Vol. 121, No. 1, 1988, pp. 135–147.

[35]Miller, I., and Freund, J. E., *Probability and Statistics for Engineers*, Prentice–Hall, Englewood Cliffs, NJ, 1965, Chap. 12.

[36]Coleman, H. W., and Steele, W. G., *Experimentation and Uncertainty Analysis for Engineers*, Wiley, 1989, Chap. 2.

[37]Krothapalli, A., Hsia, Y., Baganoff, D., and Karamcheti, K., "The Role of Screech Tones in Mixing of an Underexpanded Rectangular Jet," *Journal of Sound and Vibration*, Vol. 106, No. 1, 1986, pp. 119–143.

[38]Gutmark, E., Schadow, K. C., and Bicker, C. J., "Near Acoustic Field and Shock Structure of Rectangular Supersonic Jets," *AIAA Journal*, Vol. 28, No. 7, 1990, pp. 1163–1170.

[39]Raman, G., and Rice, E. J., "Instability Modes Excited by Natural Screech Tones in a Supersonic Rectangular Jet," *Physics of Fluids*, Vol. 6, No. 12, 1994, pp. 3999–4008.

K. Kailasanath
Associate Editor